Covert cavitation: Spectral peak suppression in the acoustic emissions from spatially configured nucleations

Jae Hee Song
Cavitation Laboratory (CavLab), Medical and Industrial Ultrasonics, School of Engineering, University of Glasgow, Glasgow, G12 8QQ, United Kingdom
JaeHee.Song@glasgow.ac.uk

Kristoffer Johansen
Cavitation Laboratory (CavLab), Medical and Industrial Ultrasonics, School of Engineering, University of Glasgow, Glasgow, G12 8QQ, United Kingdom
k.johansen.1@research.gla.ac.uk

Paul Prentice
Cavitation Laboratory (CavLab), Medical and Industrial Ultrasonics, School of Engineering, University of Glasgow, Glasgow, G12 8QQ, United Kingdom
Paul.Prentice@glasgow.ac.uk

Running title: Covert cavitation

Abstract

Dual laser-nucleation is used to precisely configure two cavitation bubbles within a focused ultrasound field of f_0 = 692 kHz, in proximity to the tip of a needle hydrophone. With both bubbles responding in the $f_0/2$ sub-harmonic regime, confirmed via ultra-high speed shadowgraphic imaging, an emission spectrum with no sub-harmonic content is demonstrated, for an inter-bubble spacing $\approx \lambda_0$. A spectral model for periodic shock waves from multiple nucleations demonstrates peak suppressions at $nf_0/2$ when applied to the experiment, via a windowing effect in the frequency domain. Implications for single-element passive detection of cavitation are discussed.

PACS numbers: 43.35.Ei

Keywords: Cavitation, spectrum, sub-harmonic suppression, periodic shock waves

1. Introduction

The emission of sub-harmonic signals from a medium during exposure to intense ultrasound, is held to be exclusive to the presence of acoustic cavitation-bubble activity within that medium. Indeed, detection at the sub-harmonics, particularly $f_0/2$ and higher-harmonics at $nf_0/2$, where f_0 is the frequency of the acoustic driving, is regularly used to determine the onset of cavitation-mediated effects in medical[1, 2] and industrial applications.[3, 4] Broadband emissions, which can assessed between spectral peaks,[5] or over frequencies sufficiently greater than f_0,[6] is also commonly used as an indicator for inertial cavitation.

We recently reported optical imaging and acoustic detection of single stable-inertial cavitation events at high temporal resolution,[7] initiated via the laser-nucleation technique[8] and driven by high-intensity focused ultrasound (HIFU). Shadowgraphic imaging facilitated via synchronous pulsed-laser illumination, revealed periodic shock waves (PSWs) emitted at f_0/m (where m is an integer value) from the bubble activity, dependent on the pressure amplitude of the driving. Detector deconvolution from the acoustic data allowed reconstruction of the PSWs, and their contribution to the cavitation spectrum to be quantitatively analyzed, validating a spectral model that suggested PSWs generate features at nf_0/m, for all values of n and m (where n is an integer value). The results indicated that PSWs were predominantly responsible for all features of the cavitation noise spectrum, other than ~15 dB at f_0, attributable to linear scattering of the driving field.

In this Letter, we describe an extension to the experimental capability such that two acoustic cavitation events can be simultaneously nucleated, in predetermined spatial configurations relative to each other, the tip of a needle hydrophone and HIFU focus. We present ultra-high speed shadowgraphic imaging to confirm that both resulting cavitation-bubbles are responding in the $f_0/2$ regime, yet the spectrum of the combined acoustic emissions reveals no perceptible sub-harmonic content, or higher harmonics of the sub-harmonic. The spectral model for PSWs is extended to account for a multi-nucleated system.

2. Experimental arrangement

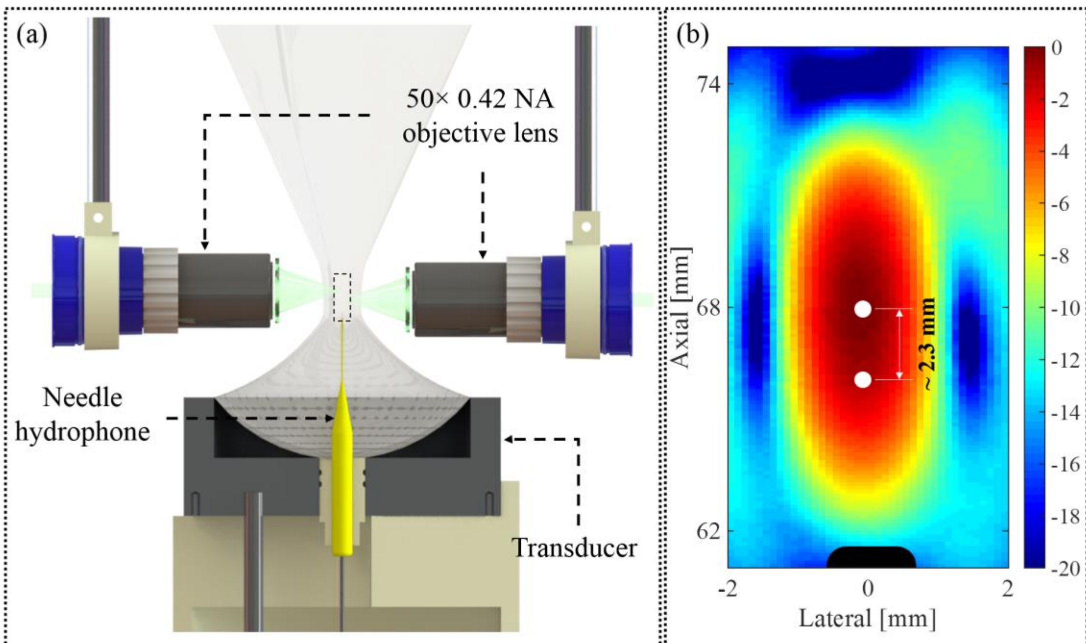

Fig. 1. (Color online) Illustration of experimental setup: (a) cross-sectional view of HIFU transducer-NH configuration, and two long-working distance objective lenses facilitating dual-laser nucleation of cavitation bubbles. (b) An axial scan of the HIFU focal region, including the targeted laser-nucleation zones, to which the nucleating laser foci were aligned.

The experimental arrangement is broadly similar to that described in detail in our previous report,[7] with two modifications distinguishing the current work. Briefly, a single element piezoceramic transducer (H-149, Sonic Concepts, Bothell, WA), generates a 90-cycle burst of HIFU at f_0 = 692 kHz and peak-positive pressure amplitude, $PPPA_{HIFU} \cong 1.63 \pm 0.12$ MPa, which drives cavitation at the focus in the $f_0/2$ regime.[7] A needle hydrophone (NH, 1.0 mm diameter, PVdF, Precision Acoustics, Dorchester, UK), calibrated for magnitude and phase over a bandwidth of 125 kHz to 20 MHz, in 25 kHz increments[9] (National Physical Laboratory, Teddington, UK, 2016), is mounted within a central hole through the body of the HIFU transducer, such that it aligns to the propagation axis of the field generated, Fig. 1 (a) and (b). Steps taken to measure the HIFU amplitude with the NH in the inverted position, Fig. 1 (a), which may be expected to perturb the field are described in detail.[7]

Cavitation is introduced to the focus of the HIFU field via the laser-nucleation technique.[8] To generate the results presented below, however, a 50:50 beam splitter (BS010, Thorlabs, Ely, UK) is introduced to the nucleating laser-pulse beam path. The component beams from a 2.4 ± 0.2 mJ (instrument error according to manufacturer), 6–8 ns laser pulse (Nano S 130-10 frequency doubled Q-switched Nd:YAG, Litron Lasers, Rugby, UK), are steered to the back apertures of two long-working distance microscope objective lenses (50× 0.42 NA Mitutoyo, Kawasaki, Japan), Fig. 1 (a), sealed in water-tight units and mounted on xyz manipulators. This configuration permits simultaneous dual laser-nucleation of two, independently positioned, cavitation-bubbles, Fig. 2.

Ultra-high speed imaging is undertaken at 5×10^6 frames per second (fps) with a Shimadzu HPV-X2 camera (Shimadzu, Kyoto, Japan), with 256 frames per sequence. Synchronous 10 ns laser pulses (CAVILUX Smart, Cavitar, Tampere, Finland) provide the illumination and effective temporal resolution, per frame. A macro-objective lens (Zeiss 100mm f2 Makro-Planar Milvus

ZF.2, Oberkochen, Germany) facilitates a larger field of view than that reported previously,[7] such that HIFU propagation as well as shock wave emission from cavitating bubbles, can be visualized.[10]

3. Results

3.1 High-speed imaging

Figure 2 depicts representative images extracted from a high-speed sequence of dual-nucleated acoustic cavitation activity, each comparable to the single bubble $f_0/2$ regime activity reported previously,[7] characterized by stable $f_0/2$ PSW emission. At the field of view delivered by the macro-objective, the bubble activity is barely resolved. However, the compressional and rarefactional phases of the propagating HIFU can be appreciated,[10] as fringes slightly brighter and darker than the ambient background (labelled C and R, Figure 2), respectively. The effect is better perceived from the movie version of the data, Mm.1, where it can also be seen that the bubbles collapse and emit shockwaves in response to every other compressional phase, confirming the $f_0/2$ response regime. The salient features of this data are two cavitating bubbles (hereafter referred to as top^t and bottom^b bubbles), separated by 2.3 ± 0.1 mm, which compares to the HIFU wavelength, $\lambda_0 = 2.14$ mm, emitting $f_0/2$ PSWs approximately in-phase. Intuitively, this leads to a combined effective shock wave detection frequency of f_0, at the NH tip, visible to the bottom of each image, Fig. 2.

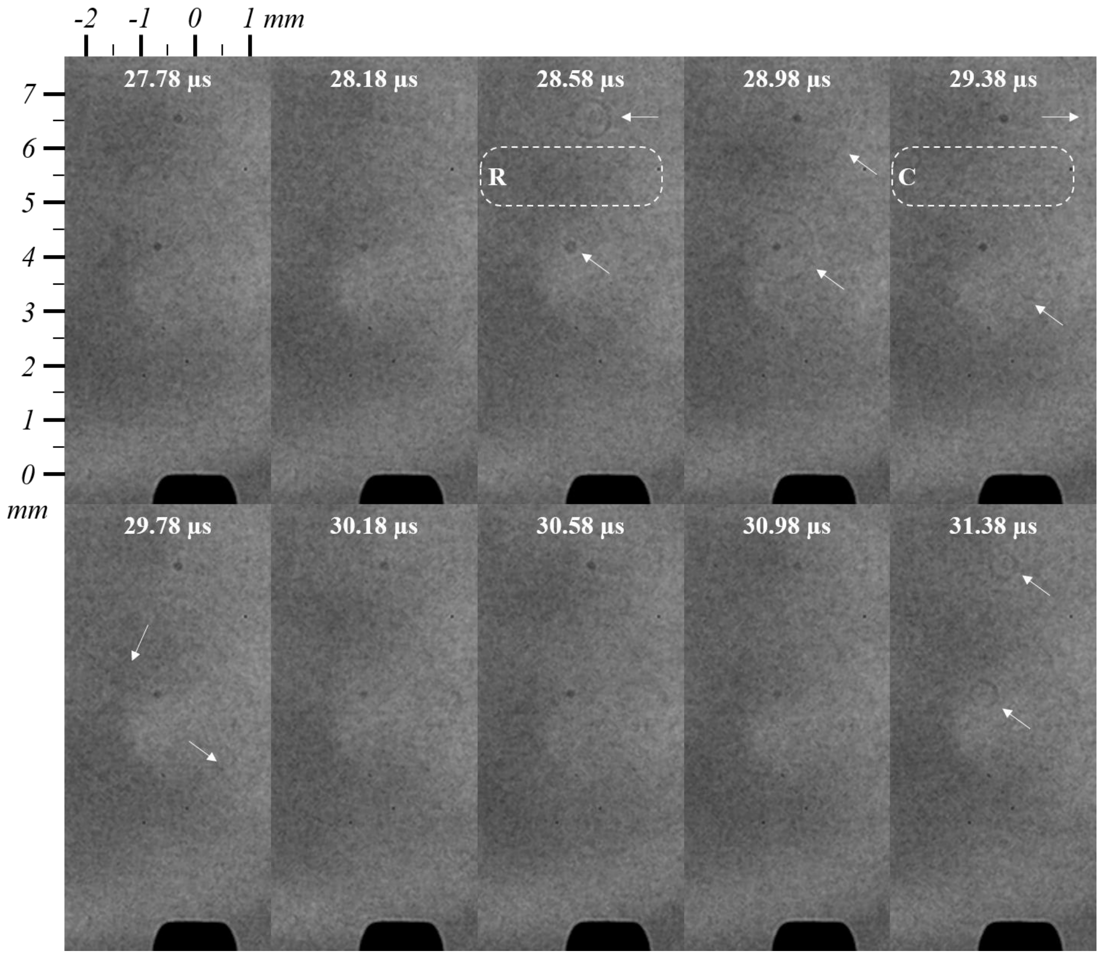

Fig. 2. Selected high-speed shadowgraphic images from Mm. 1, recorded at 5×10^6 fps, of two cavitation-bubbles with an inter-bubble spacing $\approx \lambda_0$. Transitory brighter and darker regions, imposed over an already inhomogeneous background illumination, such as indicated by dash box C and R, represent compressional and rarefactional phases of the HIFU driving. The propagating HIFU can be better perceived in the movie version of the data Mm. 1. PSW emission, arrowed at 28.58 µs and 31.38 µs (but not 30.18 µs, when an intervening compressive phase is incident) verifies that both bubbles are in the $f_0/2$ sub-harmonic regime.

Mm. 1. Movie of the entire image sequence represented in Fig. 2, at full field of view, showing in phase $f_0/2$ PSW emission from both bubbles. Video duration is 20s, file type "avi" (1.74 MB).

3.2 Hydrophone data

Figures 3 (a) and (b) (solid grey) represent the needle hydrophone data collected during the cavitation activity represented in Fig. 2, deconvolved from the impulse response of the hydrophone with magnitude and phase calibration. A HIFU control exposure, for which a burst of identical parameters was generated, but no cavitation nucleated, has also been subtracted.

A synthetic PSW signal (red dot, Figs. 3 (a) and (b)), is constructed from simulated shock wave profiles, derived from solving the Gilmore equation for a freely collapsing resonant bubble, and fitted to the experimental data.[7] Synthetic acoustic f_0 and $2f_0$ components from both bubbles in combination, of amplitudes and phases 10.68 ± 0.62 kPa, 121.75° ± 5.31° and 1.88 ± 0.52 kPa and 52.59° ± 21.96°, respectively, can be added for consistency with the full synthetic spectrum construction procedure described previously.[7] This yields a cross correlation coefficient of 0.96 between the full synthetic and experimental spectra (solid grey, Fig. 3 (c)), indicating the signal is well represented. However, for the purpose of developing the model below to derive a window function in the frequency domain, we consider only the PSW spectra (red dot, Fig 3. (c)) of the synthetic PSW signal, which presents peaks at all relevant frequency values.

Inspection of the PSW profiles of Fig. 3 (b), demonstrates that the shock waves from the top and bottom bubbles can be distinguished by their full-width at half maximum (FWHM), with the wider shocks from the lower bubble, detected at 31.66 and 34.37 μs, due to the more oblique incidence to the NH tip. Bandpass filtering of the experimental deconvolved and control-subtracted NH signal, Fig. 3 (a), from 1.5 to 20 MHz to remove f_0 and $2f_0$ components within the NH calibration range, reveals detected shock widths of $FWHM^{t}_{PSW}$ = 40.57 ± 3.97 and $FWHM^{b}_{PSW}$ = 65.00 ± 7.62 ns from the top and bottom bubbles, respectively.

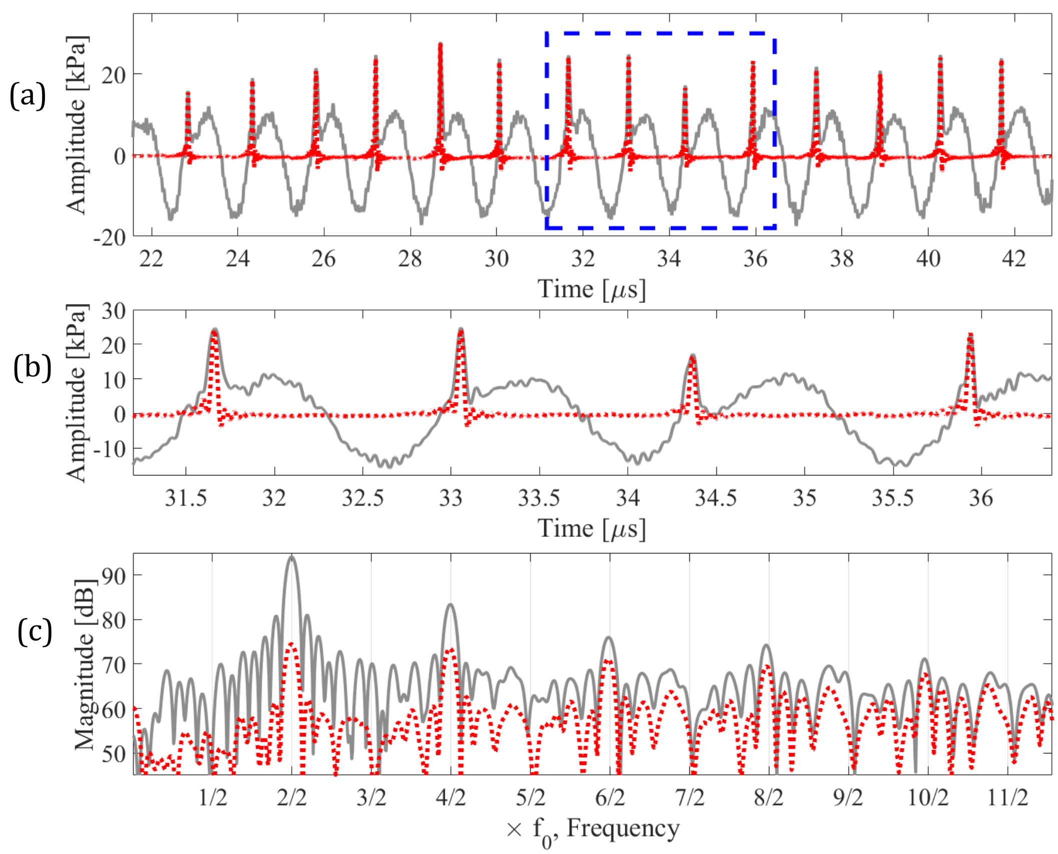

Fig. 3. (Color online) (a) Pressure-time waveforms of control-subtracted and deconvolved NH data (solid grey) and synthetic PSW signal (red dot), with the blue-dash box reproduced in (b) corresponding directly to the selected images of Fig. 2. (c) The experimental NH (solid grey) and PSW synthetic (red dot) spectra for the combination system, revealing no sub-harmonic content including at odd-numbered higher harmonics.

Analysis of Fig. 3 (a) also reveals that the period of shock wave emission, T^{t}_{PSW} = 2.893 ± 0.068 μs and T^{b}_{PSW} = 2.905 ± 0.116 μs, compared to $2T_0$ = 2.890 μs, for the HIFU field.

4. Spectral analysis model for dual bubbles

To analyze the effect on the spectrum of the combined emissions from the dual cavitation-bubble system represented in Fig. 2, we consider the synthetic PSW signal that would be detected by the NH from both bubbles, $x^{NH}_{PSW}(t)$, as the sum of the synthetic PSW signals from the top bubble, $x^{t}_{PSW}(t)$, and bottom bubble, $x^{b}_{PSW}(t)$, emitted in isolation from the other. The effects of bubble-bubble interactions, which will be particularly prevalent at smaller inter-bubble distances, are discussed below. $x^{t}_{PSW}(t)$ and $x^{b}_{PSW}(t)$ are deduced from the distinct shock wave profile FWHMs apparent from Fig. 3 (b), in combination with the high speed image sequence of the activity, such that each shock wave and its source bubble is individually identified. As both bubbles are responding to the HIFU in the same $f_0/2$ sub-harmonic regime, $x^{t}_{PSW}(t)$ can be approximated in terms of $x^{b}_{PSW}(t)$, as

$$x^{t}_{PSW}(t) \approx r \cdot x^{b}_{PSW}(t-\tau) \quad (1)$$

where r is the ratio of peak-positive pressure amplitudes $PPPA^{t}_{SW}\colon PPPA^{b}_{SW}$, of the PSWs from the top and bottom bubbles, respectively, and τ is the difference in propagation time from each bubble, to the NH tip. The frequency spectrum of the combined PSW signal detected by the NH, $X^{NH}_{PSW}(f) = \mathcal{FT}\{x^{NH}_{PSW}(t)\}$, where $\mathcal{FT}\{\cdot\}$ is the Fourier transform, can therefore be expressed in terms of the magnitude of the PSW spectrum from the bottom bubble, as

$$|X_{PSW}^{NH}(f)| \approx |1 + r \cdot cos(2\pi f \tau)| \cdot \left|X_{PSW}^{b}(f)\right| \quad (2)$$

The $[1 + r \cdot cos(2\pi f \tau)]$ term of Eq. (2) acts as a "periodic windowing" function to the magnitude response of the PSW spectrum of the bottom cloud, to obtain magnitude of the NH spectrum, $|X_{PSW}^{NH}(f)|$. τ thus determines the spacing of the window suppressions in the frequency domain, with r determining the degree of suppression. To apply the model to the dual-bubble cavitation system of Fig. 2, values are ascertained for the windowing parameters as τ = 1.444 ± 0.074 μs, and r = 1.07 ± 0.18 (with $PPPA_{SW}^{t}$ = 22.92 ± 2.20 kPa and $PPPA_{SW}^{b}$ = 21.91 ± 4.29 kPa). The resulting window function (solid blue, Fig. 4) imposed to the synthetic PSW spectrum, $X_{PSW}^{b}(f)$ (red dot), of the bottom bubble, generates the PSW spectrum as detected by the NH from the dual-bubble system, $X_{PSW}^{NH}(f)$ (solid red).

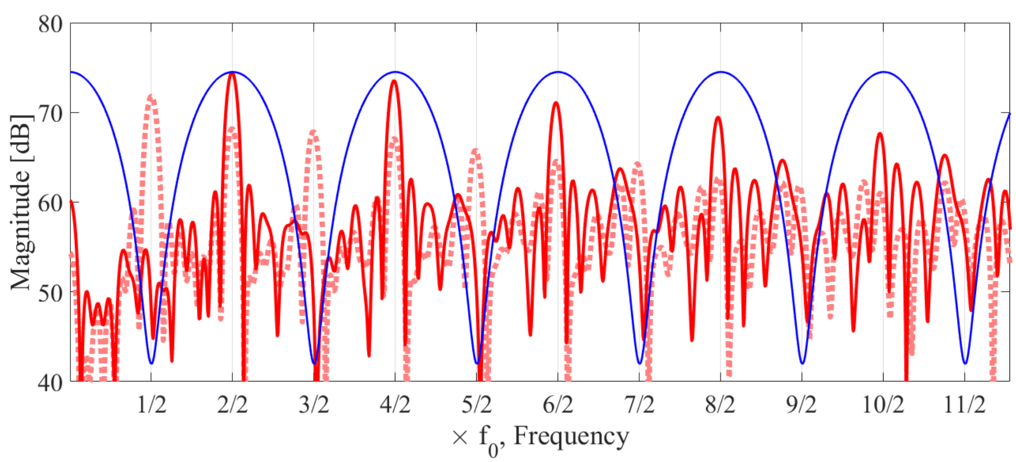

Fig. 4. (Color online) The magnitude of the synthetic *f0/2* PSW spectrum, $\left|X_{PSW}^{b}(f)\right|$, expected from the bottom bubble only (red dot), the windowing function (solid blue) with *r* and τ deduced from the experimental NH data, and the resulting NH PSW spectrum, $|X_{PSW}^{NH}(f)|$ (solid red), on application of the window.

Figure 4 confirms that $X^{b}_{PSW}(f)$, in isolation, generates peaks at all values of $nf_0/2$, including the sub-harmonic and its higher harmonics, and f_0 and its higher harmonics, consistent with our previous report.[7] In applying the window function of Eq. (2), to deduce the PSW spectrum from the dual-bubble system, however, all spectral content at $nf_0/2$ for odd-values of n, are suppressed, in line with the experimental spectrum of the dual-bubble emissions, collected by the NH, (solid grey, Fig. 3 (c)).

5. Discussion

With this experiment, we have definitively demonstrated that a medium can host cavitation activity, of a particular regime, and yet appear not to generate the acoustic signals specifically associated with that regime. In the particular example presented, the cavitation sub-harmonic at $f_0/2$, and its higher harmonics, which are signals widely used to infer the very existence of acoustic cavitation,[1-4] are significantly suppressed for any detector aligned to the HIFU axis. A windowing function is analytically expressed to predict the frequency values at which peak suppressions will occur for the spectrum of the dual-bubble cavitation activity, in terms of the PSW spectrum from one of the component bubbles. This confirms suppression at $nf_0/2$, for odd values of n, as seen in the experimental results. Moreover, the resulting signal enhancement, at even values of n (harmonics of f_0), could easily be misinterpreted as due to nonlinear HIFU propagation, rather than cavitation activity.

From Fig. 2, the distance between the hydrophone tip and the top and bottom bubbles is 6.6 and 4.3 ± 0.1 mm, respectively. Fig. 3 (b) indicates that the maximum instantaneous amplitude of the emissions from each bubble ≈ 30 kPa. Assuming the pressure amplitude decays in inverse proportion to the propagation distance, the highest instantaneous pressure within the emissions from the source bubble, at the location of the second bubble, is ~ 100 kPa. The analysis therefore assumes that the emissions from either bubble are dominated by the HIFU driving, and not significantly influenced by the other bubble, for the short duration of ~ 20 μs over which they are sampled. For extended driving durations, and smaller inter-bubble distances, bubble-bubble interactions will become significant. For example, secondary radiation force-induced translation, which is not perceptible within the high speed imaging of Fig. 2 and Mm. 1, would lead to windowing parameters that are also a function of time.

The model easily allows other configurations of two $f_0/2$ bubbles to be considered, under the assumption that they can be considered as two independent sources. If the bubbles, emitting PSWs in phase, were configured orthogonally to the HIFU propagation axis, at an inter-bubble spacing of λ_0, the shock waves from each bubble would arrive at the hydrophone tip, at the same time. The magnitude of the $f_0/2$ peak would therefore be double that from either bubble, emitting individually. Alternatively, an inter-bubble spacing of $\lambda_0/2$, along the HIFU propagation axis, will result in an effective shock wave detection frequency of $2f_0$ at the hydrophone. This would halve the value of τ used above, doubling the frequency values at which suppression occurs, such that odd-order f_0 harmonics (f_0, $3f_0$, $5f_0$, $7f_0$…) are suppressed.

More than two bubbles responding in the same regime would result in additional r and τ values, and more complex periodic windowing functions, of variable frequency spacing and degrees of suppression. For multiple cavitation-bubbles responding to an insonation in different sub-harmonic regimes, such as for a HIFU field with bubbles simultaneously within the focus and also outside of it, the windowing function cannot be analytically derived. However, the presented model may be applicable for combinations of f_0/n and f_0/m (where $n \neq m$) bubbles within limited frequencies, if they have common spectral peaks at $k \cdot L \cdot f_0$ where $k \in \mathbb{N}$, and L is the least common multiple of *1/m* and *1/n*. By taking the approximation that $X_{PSW}^{b}(f) \approx r' \cdot X_{PSW}^{t}(f)$ where $r' = r \cdot m/n$ and $f = k \cdot L \cdot f_0$, constructive and destructive interference at specific spectral peaks may be anticipated.

Evidently, the precision of laser-nucleation has allowed us to spatially configure bubble activity for maximum effect, to demonstrate spectral windowing and peak suppression. The near-complete suppression, demonstrated here for $f_0/2$ because the shock wave amplitude ratio, $r \approx 1$, of any peak would not be expected for experiments involving spontaneous and stochastically distributed cavitation. We also note that the experimental results presented above have been selected from a longer data set, as an ideal case in terms of shock wave amplitude and periodicity, to demonstrate the effect. Generally, however, care should be taken with gauging the level of cavitation activity from the magnitude of any single spectral peak.

A second detector, aligned orthogonally to the one in the configuration described here, would certainly be expected to detect sub-harmonic signal. This would indicate that multiple, spatially configured cavitation detectors would yield reliable, and reproducible measurements for correlation of cavitation-mediated effects, particularly for systems where a low number of nucleations may be anticipated. Parallel assessment of cavitation emissions over a sufficiently large bandwidth will also minimize the effects of spectral windowing.

Acknowledgements

The research leading to these results has received funding from the European Research Council under the European Union’s Seventh Framework Programme (FP/2007 – 2013)/ERC

Grant Agreement no. 336189 (TheraCav). The authors acknowledge Miriam Jiménez García for technical assistance.

References

[1]C. M. Schoellhammer, A. Schroeder, R. Maa, G. Y. Lauwers, A. Swiston, M. Zervas, R. Barman, A. M. DiCiccio, W. R. Brugge, D. G. Anderson, D. Blankschtein, R. Langer, and G. Traverso, "Ultrasound-mediated gastrointestinal drug delivery," Sci. Transl. Med. **7**, 310ra168 (2015).

[2]M. A. O'Reilly and K. Hynynen, "Blood-Brain Barrier: Real-time feedback-controlled focused ultrasound disruption by using an acoustic emission-based controller," Radiology **263**, 96-106 (2012).

[3]K. Kawabata and S. Umemura, "Use of second-harmonic superimposition to induce chemical effects of ultrasound," J. Phys. Chem., **100**, 18784-18789 (1996).

[4]H. Hasanzadeh, M. Mokhtari-Dizaji, S. Z. Bathaie, and Z. M. Hassan, "Evaluation of correlation between chemical dosimetry and subharmonic spectrum analysis to examine the acoustic cavitation," Ultrason. Sonochem., **17**, 863-869 (2010).

[5]W. S. Chen, A. A. Brayman, T. J. Matula, and L. A. Crum, "Inertial cavitation dose and hemolysis produced *in vitro* with or without Optison," Ultrasound Med. Biol., **29**, 725-737 (2003).

[6]C. C. Coussios, C. H. Farny, G. ter Haar, and R. A. Roy, "Role of acoustic cavitation in the delivery and monitoring of cancer treatment by high-intensity focused ultrasound (HIFU)," Int. J. Hyperthermia, **23**, 105-120 (2007).

[7]J. H. Song, K. Johansen, and P. Prentice, “An analysis of the acoustic cavitation noise spectrum: The role of periodic shock waves,” J. Acoust. Soc. Am., **140**, 2494-2505 (2016).

[8]B. Gerold, S. Kotopoulis, C. McDougall, D. McGloin, M. Postema, and P. Prentice, “Laser-nucleated acoustic cavitation in focused ultrasound,” Rev. Sci. Inst. **82**, 044902 (2011).

[9]K. Johansen, J. H. Song, K. Johnston, and P. Prentice, “Deconvolution of acoustically detected bubble-collapse shock waves,” Ultrasonics, **73**, 144-153 (2017).

[10]K. Johansen, J. H. Song, and P. Prentice, “Characterising focused ultrasound via high speed shadowgraphic imaging at 10 million frames per second” IEEE Ultrasonics Symposium, Tours (2016), pp. 1-4.